Ferrimagnetic Vortex Nanorings Facilitate Efficient and Safe Deep-Brain Magnetothermal Stimulation in Freely Moving Mice

galong Li[1], Xin Qiao[2], Yu Zhao[3], Dongyan Li[1], guigen Zhang[3], Xiaoli Liu[1], Fulin Chen[1], Hongbin Lu[4], Jin Zhou[2], Changyong Wang[2], and Haiming Fan[1]

[1]Northwest University
[2]Beijing Institute of Basic Medical Sciences
[3]University of Kentucky
[4]Air Force Medical University

September 02, 2024

Abstract

Magnetothermal neuromodulation is a minimally-invasive, deep-brain accessible and tether-free technique. The precisely timed activation of thermosensitive ion channels, such as TRPV1, with local heat generated using magnetic nanoparticles is crucial for efficient neuromodulation. Nevertheless, this technique is greatly hindered by its long stimulus-response time and high safety risks due to the poor heat-generating performance of the nanomediators. Herein, we report the establishment of a ferrimagnetic vortex iron oxide nanoring (FVIO)-mediated magnetothermal neurostimulation technique that is efficient and safe. Compared with widely used superparamagnetic iron oxide nanomediators (SPIOs), the FVIOs triggered Ca2+ influx into HEK293T cells and cortical neurons at an Fe concentration of 54 μg/mL, which is 20.27-fold lower than that needed for SPIOs. In vivo magnetothermal stimulation in the central nucleus of the amygdala of mice further demonstrated that FVIOs with the optimal dose of 0.05 μg evoked fear behaviors with an average latency of 2.51 s, which was 2.3-fold faster than that in the SPIO (0.8 μg)-treated group. More importantly, FVIOs-mediated stimulation not only exhibited negligible histopathological alterations and proinflammatory cytokine expression, but also successfully elicited fear behaviors in transgene-free mice. The FVIO-mediated efficient and safe neuromodulation has the potential for future neuroscience exploitation and neurological disease treatment.

Introduction

Magnetothermal neurostimulation is emerging as a powerful technique for gaining insight into intricate brain circuits and performing therapeutic investigations of neurological disorders given its distinct advantages, such as minimal invasiveness, tether-free operation, deep brain accessibility, and high spatial resolution[1-2]. In this technique, biocompatible magnetic nanoparticles are utilized as nanoheaters to generate heat locally through the hysteresis loss process under alternating magnetic fields (AMFs)[3]. The increase in local temperature can activate the thermosensitive ion channels that are overexpressed on the cell membrane and trigger an influx of calcium (Ca^{2+}) into neurons, thereby modulating neural activity[4]. To date, magnetothermal neurostimulation has been demonstrated to bidirectionally modulate neuronal activity[5-8], successfully regulate blood glucose[9-10] and adrenal hormone levels in vivo[11], and control the motor behaviors of worms[8, 12], flies[13] and freely moving mice[14]. However, current techniques still suffer from low activation efficiency and high required dosages of nanoheaters, leading to an unexpectedly long stimulus-response time and potential safety concerns[13].

According to the principles of magnetothermal neurostimulation, the precisely timed activation of a single neuron depends on both the expression level of thermosensitive ion channels and the heating efficiency of the nanoparticles under an AMF[11, 15-16]. Transient receptor potential cation channel subfamily V member

1 (TRPV1), the thermosensitive ion channel most commonly used in neuromodulation, can be activated by local heat (> 43 °C)-induced conformational changes in the channel pore[17-20]. Moreover, the rate of TRPV1 opening increases exponentially with increasing surrounding temperature[19, 21]. Because an increase in TRPV1 expression in vivo requires viral vector-mediated gene transfection, which comes with high safety risks, the key to quickly and safely activating TRPV1 lies in boosting the heat-generating performance of magnetic nanoparticles[3-4, 11]. Unfortunately, the superparamagnetic iron oxides (SPIOs) and ferritin protein widely used in magnetothermal neurostimulation show poor thermal conversion efficiency due to their superparamagnetic nature and minimal hysteresis loss[22-25]. In addition, an AMF with a high amplitude (H) and frequency (f) is frequently needed to improve the heat-generating ability of the nanoheater[26-28]. Nevertheless, less improvement has been achieved because of the biologically acceptable limit (H $\times f$ [?] 5 x 10^9A/(m*s))[28-30]. Recognizing the above limitations, developing a high-performance magnetic nanoparticle-mediated stimulation technique is a valuable approach for realizing efficient and safe magnetothermal neuromodulation[31-33].

Significant efforts have been made to synthesize various magnetic nanoparticles with enhanced heat-generating performance given their wide application in magnetic hyperthermia, controlled drug delivery, cell signal transduction activation and magnetothermal neurostimulation[30, 34-39]. The thermal conversion efficiency of nanoparticles is commonly evaluated using the specific absorption rate (SAR), which mainly depends on the intrinsic magnetic properties of the nanoparticles[40-42]. Despite tuning their composition, shape, size and surface chemistry of various magnetic nanoparticles, most exhibit relatively low SAR values ranging from 250 W/g to 1000 W/g[30, 43-45]. As a result, these nanoparticles take more time to reach the threshold temperature and activate TRPV1, leading to long latency times (approximately 14.7 s) for behavior onset[13, 18, 46]. Applying a high dose of magnetic nanoparticles is an alternative method to reduce the heating time[26]. Nevertheless, using excessive amounts of nanoheaters increases the risk of nonnegligible safety issues in the brain, such as dopamine neuron damage, homeostatic disruption and inflammatory responses[47]. We previously reported that novel biocompatible ferromagnetic vortex-domain iron oxide nanorings (FVIOs) exhibit an ultrahigh SAR of greater than 3000 W/g because of their unique vortex-to-onion magnetization reversal phenomenon upon AMF exposure[48]. Notably, as our simulation results revealed, only 8.70 x 10^{-6} ng of FVIOs could effectively increase the local temperature from 37 degC to 43 degC, whereas 33.6 x 10^{-6} ng of SPIOs was needed under the same AMF conditions (Figure S1**, Supporting Information**). In addition, relatively large size and biocompatible FVIOs are more stable in the brain, which is favorable for long-term and repeated magnetothermal neurostimulation in vivo[48]. As such, FVIOs are likely to be high-performance nanoheaters that facilitate quick activation of TRPV1, which might provide an opportunity to establish a highly efficient and safe magnetothermal neurostimulation technique.

In the present study, we comprehensively investigated FVIO-facilitated magnetothermal neurostimulation in vitro and in vivo, and compared the results with those of widely used SPIO-based approaches. **The newly designed FVIOs with an anti-His antibody coating triggered Ca^{2+} influx in** TRPV1-expressing HEK293T **ϲεllϲ ανδ ϲοrtιϲαl νευrονϲ ωιτη α μινιμυμ Φε ϲονϲεντρατιον οφ 54 μγ/μΛ, ωηιϲη ωαϲ 20.27-φολδ λοωερ τηαν τηατ οφ τηε ΣΠΙΟϲ** under the same AMF treatment. In vivo magnetothermal stimulation in the central nucleus of the amygdala (CeA) further demonstrated that FVIO treatment quickly evoked fear behaviors in mice, exhibiting a response time that was 2.3-fold faster than that in the SPIO-treated group. Overall, the lowest effective dose of FVIOs was 0.05 μg in vivo, 16.7 fold less than the effective dose of SPIOs. More importantly, t**he SPIO (** 0.8 μg**)-treated mice exhibited significant histopathological changes (such as vacuolar degeneration) and upregulated proinflammatory cytokine (such as interleukin-6 (IL-6)) expression in the CeA. In contrast, the FVIO (** 0.05 μg**)-treated mice showed negligible histopathological alterations and changes in proinflammatory cytokine expression. In addition,** in the FVIO-treated groups, fear behaviors were successfully induced in the mice on the 60th day after injection. However, in the SPIO-treated group, fear behaviors could not be induced on the 30th day. Notably, **ονλψ 0.28 μγ οφ Φ″ΙΟϲ αϲτιατεδ τηε ἒΑ ενδογενουϲλψ εξπρεϲϲινγ ΤΡΠ″1 ανδ ελιϲιτεδ φεαρ βεηαιορϲ ιν τρανϲγενε-φρεε μιϲε.** The aim of this work was to establish an efficient and safe FVIO-facilitated magnetothermal neuromodulation technique,

which is expected to be a powerful tool for future neuroscience investigations and therapeutic applications to neurological disorders.

Results and discussion

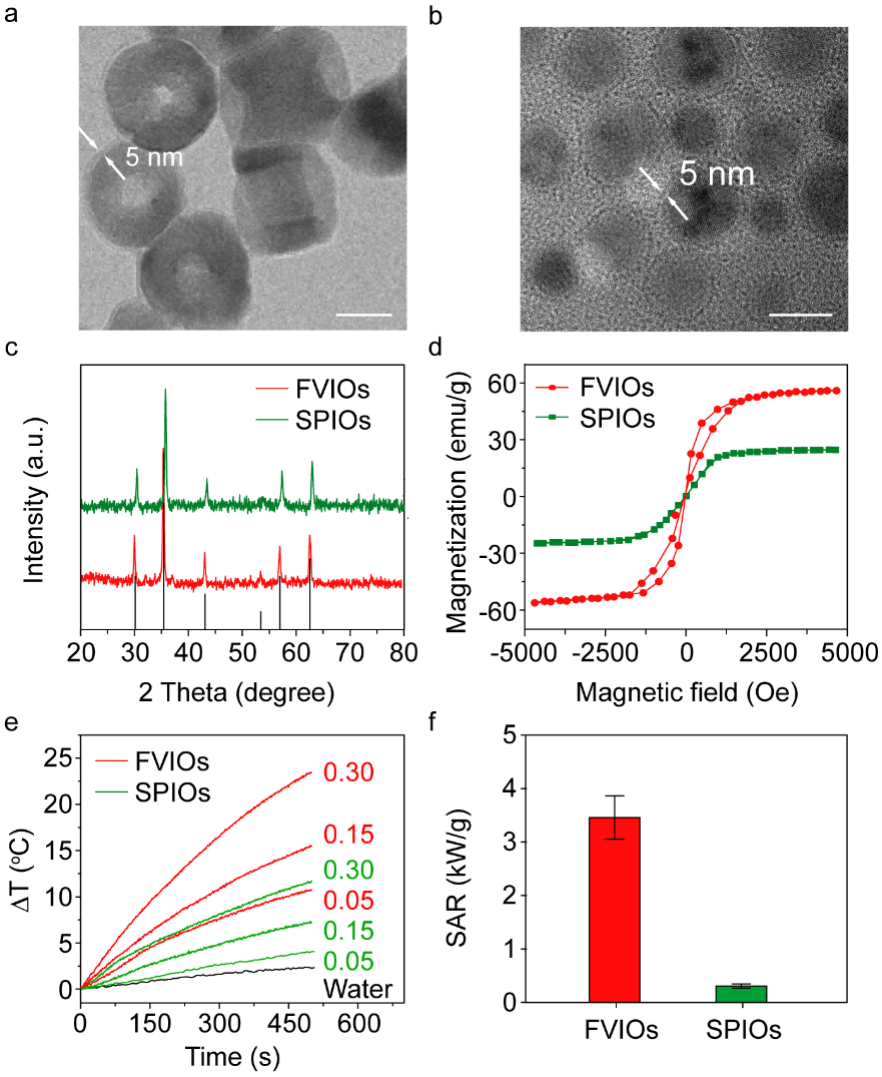

Fig. 1 Characterization of FVIOs and SPIOs. TEM images of the negatively stained (a) FVIOs and (b) SPIOs. The marked surface layer (˜ 5 nm thick) corresponds to the anti-His antibodies and DHCA coating. Scale bars, 20 nm. (c) Powder X-ray diffraction patterns of the SPIOs and FVIOs. (d) Room temperature magnetization curves constructed for SPIOs and FVIOs. (e) Temperature changes in the SPIO and FVIO solutions at various Fe concentrations (0.05, 0.15, and 0.30 mg/mL) under AMF exposure (H = 20 mT and f = 275 kHz). (f) The specific absorption rate (SAR) was calculated from the rate of temperature increase of the SPIO and FVIO solutions. The data are presented as the mean ± S.D.; n = 3 independent experiments for each sample.

In vitro magnetothermal activation of TRPV1-expressing cells

To precisely evaluate the efficacy of FVIO-mediated magnetothermal activation of the TRPV1 channel, mo-

noclonal HEK293T cell lines were generated that stably expressed 6× His-labeled TRPV1 channels. TRPV1 was labeled with the red fluorescent protein mCherry, which was separated by the posttranscriptional cleavage linker p2A. The western blotting showed that TRPV1 fusion protein was expressed on HEK293T cells (Figure S5**, Supporting Information**). Figure 2a presents a schematic of the FVIO-mediated magnetothermal activation of TRPV1 and Ca^{2+} influx into cells. The fluorescent Ca^{2+} indicator Fluo-4 was loaded into transfected HEK293T cells to monitor the changes in the intracellular Ca^{2+} concentration in response to magnetothermal stimulation. After application of the anti-His-FVIOs targeting the TRPV1 channel, the change in green fluorescence intensity during magnetothermal stimulation was recorded in real time using confocal laser scanning microscopy (CLSM) equipped with an AMF generator (Figure S6**, Supporting Information**).

Before performing the magnetothermal activation experiments, we measured the local change in temperature around the FVIOs under an AMF (20 mT, 200 kHz) to confirm that the local heating offered by the FVIOs was sufficient to activate the TRPV1 channel. FVIOs were modified with fluoresceinamine (FL; emits green fluorescence) for use as a molecular-scale thermometer. First, the fluorescence intensity and bulk temperature increase of the FVIOs-FL dispersion were recorded during AMF exposure. The percent change in fluorescence intensity decreased linearly with increasing temperature[8], reaching –1.97 ± 0.04%/°C for FL (Figure S7**, Supporting Information**). On this basis, FVIOs-FL were used to target the TRPV1 channels expressed on cultured HEK293T cells (Figure 2b; Figure S8**, Supporting Information**), and the change in FL fluorescence intensity was measured upon AMF exposure. The local temperature changes near the FVIOs were calculated according to the linear temperature-fluorescence intensity curve. After 30 s of AMF exposure, the local temperature in the immediate vicinity of TRPV1 on the cell membrane increased from 36 to 43 °C and then decreased rapidly to 36 °C in the absence of an AMF (Figure 2c). A local temperature increase to more than 43 °C near the FVIOs is sufficient to activate the TRPV1 channel by inducing a conformational change in the protein. In addition, the simulation results revealed that the local temperature decreases as the distance between the surface of a single FVIO and water increases (Figure S9a**, Supporting Information**). No heat was generated in the cell culture media according to the infrared thermal images (Figure S9b**, Supporting Information**).

FVIO-mediated magnetothermal activation of TRPV1 was systematically investigated through in situ Ca^{2+} imaging in cultured 293T cells, where Ca^{2+} influx indicates the opening of the TRPV1 channel and increased cellular activity. The fold changes in the intracellular fluorescence intensity (F_t/F_0) of the Ca^{2+}indicator Fluo-4 were recorded under different experimental conditions. Intense green fluorescence corresponding to the intracellular Ca^{2+} signal was observed upon AMF exposure. After treatment with anti-His-FVIOs, the $F_t/F_0$of the TRPV1-expressing HEK293T cells increased with prolonged AMF exposure, which was attributed to successful heat-triggered Ca^{2+} influx, as shown in Fig. 2 (d and e). This increase in fluorescence induced by Ca^{2+} influx was observed only in TRPV1-expressing cells that were activated by anti-His-FVIOs-mediated magnetothermal stimulation and in the group treated by agonist capsaicin (CAP, 10 μM). The cells in the negative control group, were cultured in **media containing the antagonist capsazepine (CZP,** 5 μM**), and** no significant difference in fluorescence intensity was observed during anti-His-FVIO-mediated magnetothermal stimulation**. Moreover,** the control groups, including the TRPV1 no expressing group, the FVIO-treated group and the AMF-treated group, exhibited negligible**Ca^{2+}-dependent changes in fluorescence intensity** .

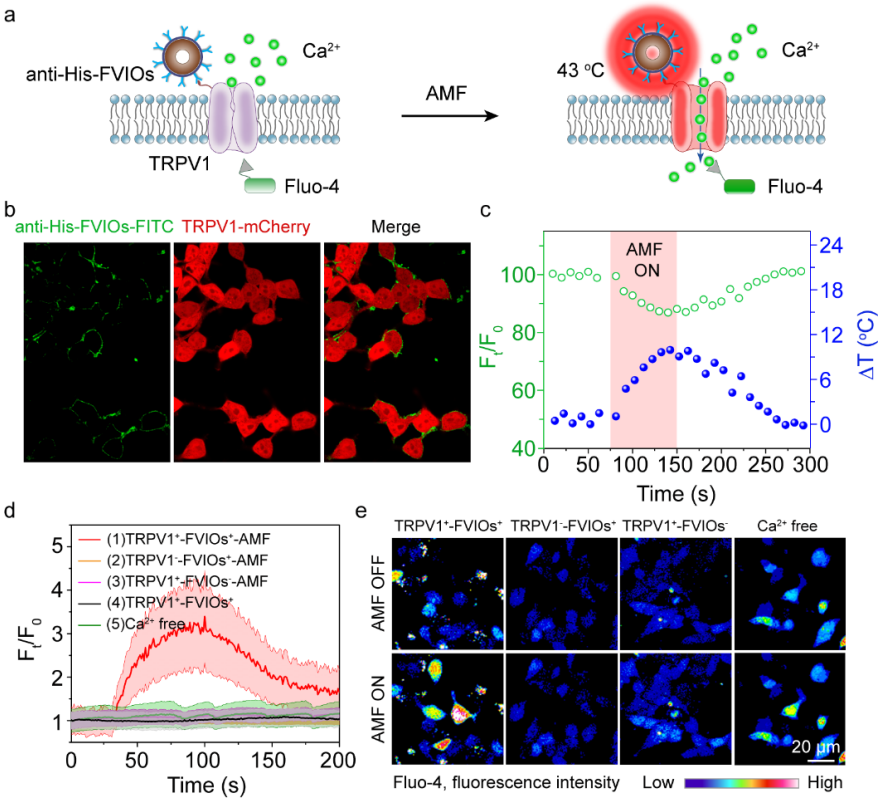

Fig. 2 In vitro magnetothermal activation of TRPV1 triggers Ca^{2+} influx. (a) Schematic of FVIO-mediated magnetothermal activation of TRPV1 triggering of Ca^{2+}influx. Fluo-4 was used as the Ca^{2+} indicator. (b) SIM images of TRPV1-expressing HEK293T cells (red) bound to FL labeled anti-His-FVIOs (green). (c) Local temperature increase near the FVIOs upon AMF exposure determined by measuring the change in green fluorescence intensity of anti-His-FVIOs- FL target the cell membrane. (d) Fold changes in fluorescence intensity (F_t/F_0 values) and (e) color maps of Fluo-4 in HEK293T cells under different experimental conditions. TRPV1-expressing, $TRPV1^+$; TRPV1-nonexpressing, $TRPV1^-$; before AMF exposure, AMF OFF; during AMF exposure, AMF ON; with FVIOs treatment, $FVIOs^+$; without FVIOs treatment, $FVIOs^-$.; Ca^{2+} free group, $TRPV1^+$-$FVIOs^+$-AMF-Ca^{2+}-free group. AMF conditions: H = 20 mT and f = 290 kHz. The solid lines and shaded areas represent the means and standard error of the mean (SEMs), respectively, the data presented as the mean ± SEM.

We further studied the influence of the Fe concentration on the stimulus-response time and fold changes in fluorescence intensity due to Ca^{2+} influx into cells. As shown in Fig. 3a, the response time of Ca^{2+} influx into cells decreased when the Fe concentration from the anti-His-FVIOs in the HEK293T cell culture media ranged from 51 to 498 μg/mL. HEK 293T cells treated with anti-His-FVIOs at an Fe concentration of 324 μg/mL showed the fastest response in terms of Ca^{2+} influx and the greatest fold change in fluorescence intensity (Figure S3a, movie S1 **, Supporting Information**). Ca^{2+} influx into cells occurred only at an Fe concentration of 1095 μg/mL or greater in the SPIO-treated groups (Figure 3b). Notably, the minimum Fe concentration needed for TRPV1 activation was 51 μg/mL in the FVIO-treated group, which was 20.27-fold lower than that in the SPIO-treated group. This finding is consistence with our early simulation results showing that a single TRPV1 channel can be activated using a less FVIOs than SPIOs (Figure S1**, Supporting Information**). Together, this experimental evidence suggests that FVIOs with superior heat-generating performance could enable efficient magnetothermal activation of thermosensitive TRPV1 expressed on cells.

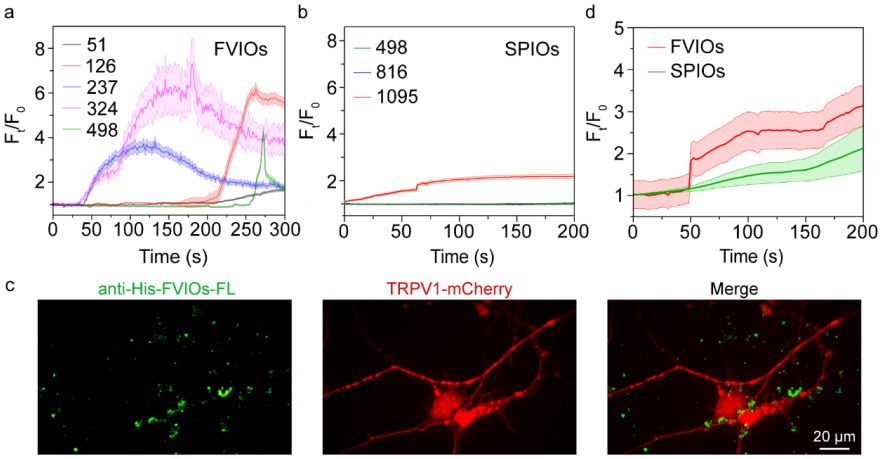

Fig. 3 In vitro magnetothermal induction of Ca^{2+} influx in TRPV1-expressing 293T cells. (a, b) Fold changes in fluorescence intensity (F_t/F_0 values) of Fluo-4 in 293T cells during magnetothermal treatment with anti-His-FVIOs at Fe concentrations ranging from 51 to 498 μg/mL, and with anti-His-SPIOs at Fe concentrations of 498, 816, and 1095 μg/mL. AMF conditions: H = 20 mT and f = 290 kHz. (c) SIM images of TRPV1-expressing cortical neurons (red) bound to anti-His-FVIO-FL (green). (d) Fold changes in fluorescence intensity (F_t/F_0 values) of Fluo-4 as a function of time for TRPV1-expressing cortical neurons treated with FVIOs (324 μg/mL) or SPIOs (1095 μg/mL). AMF conditions: H = 20 mT and f = 290 kHz. The data are presented as the mean ± SEM; the solid lines indicate the means, and the shaded areas indicate the SEMs.

We further examined Ca^{2+} influx in cultured TRPV1-expressing cortical neurons using the nanoheaters anti-His-FVIOs. FL-labeled anti-His-FVIOs **successfully** targeted **TRPV1 on cortical neurons** (Figure 3c). Moreover, the cells **were loaded with Fluo-4 to monitor Ca^{2+} influx (Figure S10, movie S2, Supporting Information). As shown in Fig. 3d, upon magnetothermal stimulation with anti-His-FVIOs at an** Fe concentration of 324 μg/mL, **α^{2+} φλυορεσϲενϲε ιν ϲορτιϲαλ νευρονϲ ραπιδλψ ινϲρεαϲεδ φρομ 50 το 200 ϲ. Ιν ϲοντραϲτ, τηε α^{2+} φλυορεσϲενϲε ιντενϲιτψ ιν νευρονϲ ινϲρεαϲεδ ϲλοωλψ ιν ρεϲπονϲε το μαγνετοτηερμαλ ϲτιμυλατιον βψ τηε αντι-Ηιϲ-ΣΠΙΟϲ ατ αν Φε ϲονϲεντρατιον οφ 1095 μγ/μΛ. Τηερεφορε, τηε αντι-Ηιϲ-Φ″ΙΟ νανοηεατερ ιϲ βελιεεδ το εναβλε εφφιϲιεντ μαγνετοτηερμαλ νευραλ αϲτιατιον ατ λοω Φε ϲονϲεντρατιονϲ.**

FVIOs-mediated fast and safe magnetothermal neurostimulation in vivo

Next, we verified that anti-His-FVIO-mediated magnetothermal stimulation in vivo can efficiently and safely evoke quick behavioral responses in freely moving mice. The central amygdala (CeA) was chosen for in vivo magnetothermal deep brain stimulation because it plays a crucial role in physiological and behavioral responses to fearful stimuli[51]. And CeA has been widely used to evaluate the efficiency of various neuromodulation techniques, such as optogenetics[52]. Figure 4a schematically illustrates the process of using anti-His-FVIO-based magnetothermal neurostimulation of the CeA and fear behavior analysis of freely moving mice, whereas an adeno-associated virus was used to express a His-tagged TRPV1 and red fluorescent mCherry fusion protein in CeA mouse neurons. After viral transfection, the anti-His-FVIO suspension was injected into the CeA region. The immunohistochemical results showed that anti-His-FVIO-FL (green) colocalized with TRPV1-expressing neurons (red) in the CeA, suggesting that the anti-His-FVIOs successfully targeted TRPV1 channels (Figure 4b). After three days of recovery and habituation, the mice were transferred to a custom-made AMF generator coil equipped with a fear behavior video analysis system. An AMF apparatus

with a 6-turn coil (diameter, 12 cm) was used here to produce an AMF with amplitudes up to 20 mT at a frequency of 275 kHz, to guarantee sufficient heat generation by the FVIOs to excite the CeA regions in the deep brains of the mice.

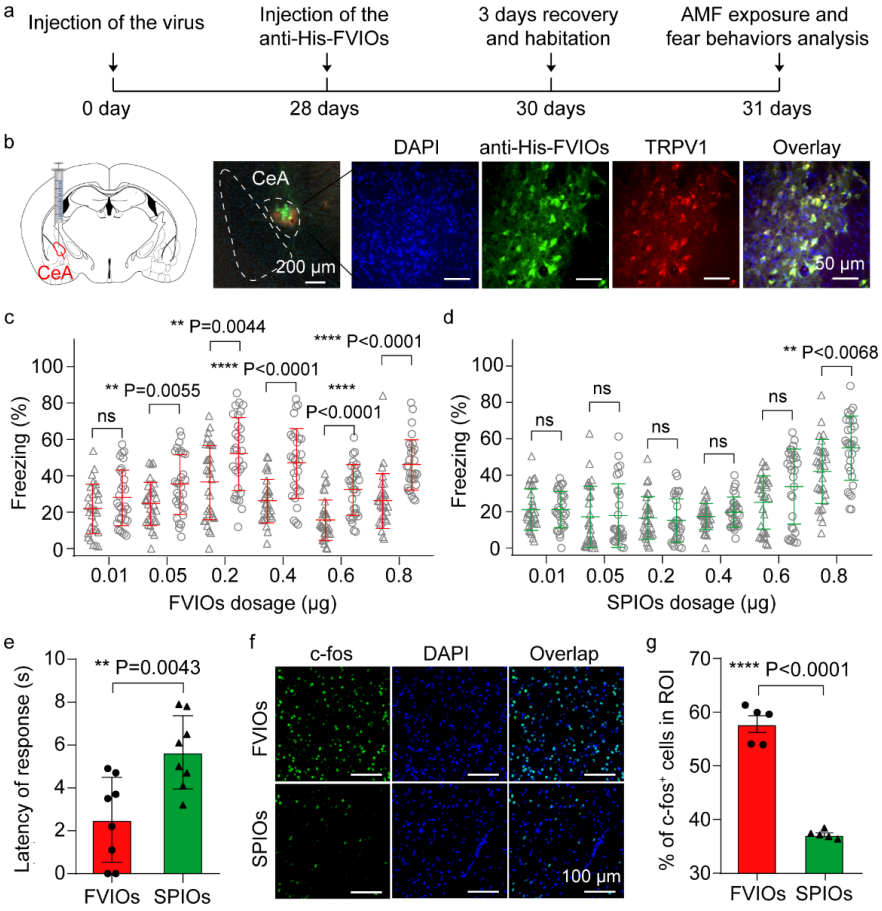

Fig. 4 Virus and FVIOs injection into the mouse CeA for the magnetothermal neuromodulation of fear behaviors. (a) Scheme of anti-His-FVIO-based magnetothermal neurostimulation of the CeA and fear behavior analysis of freely moving mice. (b) Confocal images of brain slices showing that the anti-His-FVIOs-FL (green) are located in the TRPV1-expressing CeA regions (red) of the mice. (c, d) Percentage of freezing time in mice after injection with different doses of anti-His-FVIOs (or anti-His-SPIOs) before and during AMF stimulation ($H = 20$ mT, $f = 275$ kHz)**. The black and red (or green) lines represent AMF OFF and AMF ON, respectively. One-way ANOVA was performed followed by a two-sided Student's test with thresholds. (e) Latency to the start of the first freezing episode during AMF stimulation in mice. (f) DAPI (blue), c-fos (green) and overlay confocal images of the CeA regions of mice obtained after magnetothermal stimulation. (g) Percentage of c-fos-expressing cells in the CeA among the DAPI-labeled cells. Error bars indicate the mean ± SEM, two-sided Student's t-test with the threshold ****P < 0.0001.**

Βεηαιοραλ ςηανγες ιν τηε μιςε ιν ρεσπονσε το διφφερεντ δοσες οφ τηε νανομεδιατορ ωερε ινεστιγατεδ υσινγ μαγνετοτηερμαλ αςτιατιον οφ τηε ẽA. Ας σηοων ιν Φιγ. 4ς, 0.05 μγ οφ αντι-Ηισ-Φ″ΙΟς ινδυςεδ φρεεζινγ βεηαιορ ιν μιςε ιν ρεσπονσε το ΑΜΦ απ-πλιςατιον. Τηε περςενταγε οφ φρεεζινγ τιμε ωας γρεατερ δυρινγ τηε ΑΜΦ απππλιςατιον

περιοδ τηαν δυρινγ τηε ΑΜΦ ΟΦΦ περιοδ (Φιγυρε 4ς). Ηοωεερ, νονε οφ τηε μιςε σηοωεδ φεαρ βεηαιορς ωηεν ινθεςτεδ ωιτη τηε σαμε δοσε οφ ΣΠΙΟς (Φιγυρε 4δ). Φυρτηερ στυδιες ρεεαλεδ τηατ τηε ΣΠΙΟς ςουλδ μαγνετοτηερμαλλψ εοκε σιγνιφιςαντ φρεεζινγ ρεσπονσες ονλψ ατ δοσες γρεατερ τηαν 0.80 μγ, ωηιςη ωας 16-φολδ γρεατερ τηαν τηε δοσε οφ Φ″ΙΟς νεεδεδ το ελιςιτ α ρεσπονσε. Μορεοερ, νο σιγνιφιςαντ διφφερενςες ιν φρεεζινγ βεηαιορς ωερε νοτεδ ιν τηε ςοντρολ γρουπς ωιτη ορ ωιτηουτ Φ″ΙΟ ινθεςτιον, ΑΜΦ αππλιςατιον, ανδ ΤΡΠ″1 οερεξπρεσσιον. Τηε λατενςψ το φεαρ ρεσπονσε οφ τηε μιςε ωας αλσο ρεςορδεδ το αναλψζε τηε τεμποραλ ρεσολυτιον οφ μαγνετοτηερμαλ νευροστιμυλατιον. Νοταβλψ, Φ″ΙΟ (0.05 μγ)-τρεατεδ μιςε εξηιβιτεδ α φεαρ βεηαιοραλ ρεσπονσε ωιτη αν αεραγε λατενςψ τιμε οφ 2.51 ς, ωηιςη ωας 2.3-φολδ φαστερ τηαν τηατ οφ τηε ΣΠΙΟ (0.80 μγ)-τρεατεδ γρουπ (Φιγυρε 4ε). ὃμπαρεδ ωιτη τηε πρειουσλψ ρεπορτεδ λατενςψ τιμε οφ τενς οφ σεςονδς ιν μουσε εξπεριμεντς, Φ″ΙΟ-μεδιατεδ στιμυλατιον ηας βεεν δεμονστρατεδ το βε α συπεριορ τεςηνιχυε φορ ιμπροινγ τηε τεμποραλ ρεσολυτιον οφ ιν ιο μαγνετοτηερμαλ νευρομοδυλατιον.

The magnetothermal activation of neurons in the CeA was examined using immunoanalysis of c-fos expression, which is widely used as a measure of neuronal activation. The proportion of cells expressing c-fos in the CeA was 57.78 ± 3.50% after low-dose (0.05 μg) FVIO stimulation, as shown in Fig. 4 (f and g). However, a significantly lower percentage of c-fos-positive cells (37.16 ± 0.77%) was detected in the high-dose (0.80 μg) SPIO-stimulated mice. The results suggested that FVIO-mediated magnetothermal neurostimulation can efficiently activate many more neurons in the CeA than can SPIO-mediated neurostimulation under the same conditions.

Ωε τριεδ το εσταβλιση αν οπτιμυμ Φ″ΙΟ-μεδιατεδ στιμυλατιον μετηοδ ωηιςη σατισφιες τηε νευρομοδυλατιον ρεχυιρεμεντ ωηιλε ρεσυλτινγ ιν τηε λεαστ τισσυε δαμαγε ον τηε βραιν ρεγιον[47]. Τηερεφορε, ωε φυρτηερ εαλυατεδ τηε βιοσαφετψ οφ Φ″ΙΟ-μεδιατεδ μαγνετοτηερμαλ νευροστιμυλατιον ιν μιςε, ωηιςη ις ιταλ φορ βραιν σαφετψ[53-54]. Ρεπρεσεντατιε ηεματοξψλιν ανδ εοσιν (H&E)-σταινεδ σεςτιονς φρομ Φ″ΙΟ (0.05 μγ)-τρεατεδ μιςε εξηιβιτεδ νο ηιστοπατηολογιςαλ αλτερατιονς ιν τηε ἒΑ ρεγιον (Φιγυρε 5α). Ιν ςοντραστ, ΣΠΙΟ τρεατμεντ ατ τηε μινιμυμ δοσε οφ 0.80 μγ ςαυσεδ σιγνιφιςαντ ηιστοπατηολογιςαλ ςηανγες ιν τηε ἒΑ ρεγιονς οφ τηε μιςε, ινςλυδινγ αςυολαρ δεγενερατιον ανδ νυςλεαρ ςηροματιν ςονδενσατιον ανδ φραγμεντατιον. Αφτερ μαγνετοτηερμαλ τρεατμεντ, τηε ΣΠΙΟς ινδυςεδ νευροναλ λοσς ιν τηε ἒΑ ρεγιονς οφ τηε μιςε, ας σηοων βψ Νισσλ σταινινγ. Μορε σηρυνκεν νευρονς ωιτη πψκνοτις νυςλει ωερε φουνδ ιν τηε ΣΠΙΟ-τρεατεδ μιςε τηαν ιν τηε Φ″ΙΟ-τρεατεδ μιςε (Φιγυρε 5α). Ωε φυρτηερ ασσεσσεδ ινφλαμματιον ιν τηε ἒΑ ρεγιονς οφ τηε μιςε αφτερ μαγνετοτηεμαλ νευροστιμυλατιον υσινγ ιμμυνοηιστοςηεμιςαλ αναλψσις (Φιγυρε 5β). Τηε εξπρεσσιον λεελς οφ προινφλαμματορψ ςψτοκινες (ιντερλευκιν-6 (ΙΛ-6), ΤΝΦ-α, ανδ ΙΛ-1β) ιν Φ″ΙΟ-τρεατεδ μιςε ωερε σιγνιφιςαντλψ λοωερ τηαν τηοσε ιν ΣΠΙΟ-τρεατεδ μιςε (Φιγυρε 5, ς το ε). Τηις ωας ασςριβεδ το τηε ηιγη δοσε οφ ΣΠΙΟς (0.8 μγ περ ἒΑ ρεγιον) νεεδεδ, ωηιςη ςαυσεδ υνφαοραβλε ηεατ δαμαγε ιν τηε ἒΑ ρεγιον. Τηεσε ρεσυλτς ιμπλψ τηατ Φ″ΙΟ-μεδιατεδ μαγνετοτηερμαλ νευροστιμυλατιον ις μυςη σαφερ τηαν ΣΠΙΟ-βασεδ τρεατμεντ.

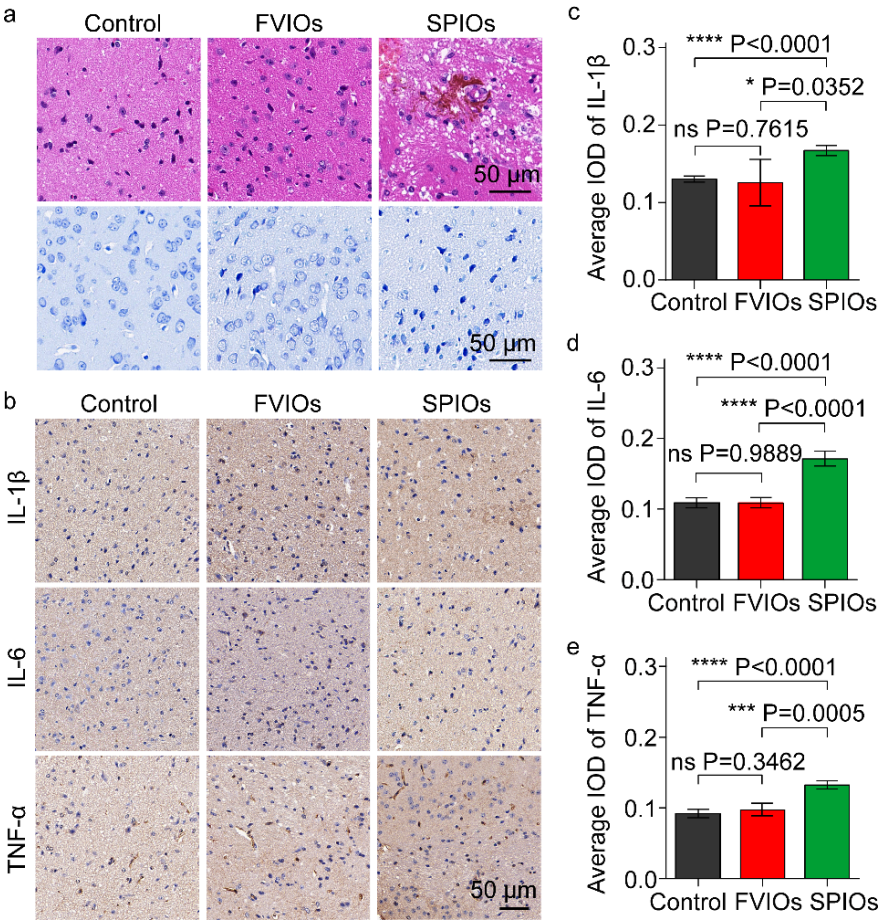

The fear behaviors induced by magnetothermal treatment in freely moving mice administered the optimal dose of FVIOs were systematically investigated using in situ video recording and further analysis according to standard protocols. Upon AMF exposure, the FVIO-stimulated mice showed freezing of gait, with locomotion inhibited in place and all four paws locked, although the mice were free to move their heads (Figure 6a). These behaviors reflected the innate anxiety and fear responses of the mice. The tracked positions and total distances traveled are displayed in Fig. 6 (b and c). The mice displayed active locomotion within the arena (coil) before stimulation. During stimulation, the mice preferentially remained frozen, showing an apparent decrease in ambulatory activities (movie S3, Supporting Information). The percentage of freezing time in the FVIO treatment mice after the application of an AMF was 79.58 ± 24.54%, which was 2.56-fold greater than that among the FVIO-treated mice without AMF exposure (Figure 6d). Before and during stimulation, the mice also exhibited significant increase in the total number of freezing episodes (from 5 to 25), which is consistent with the significant decrease in average speed (from 2.3 cm/s to 0.2 cm/s), as shown in Fig. 6 (e and f).

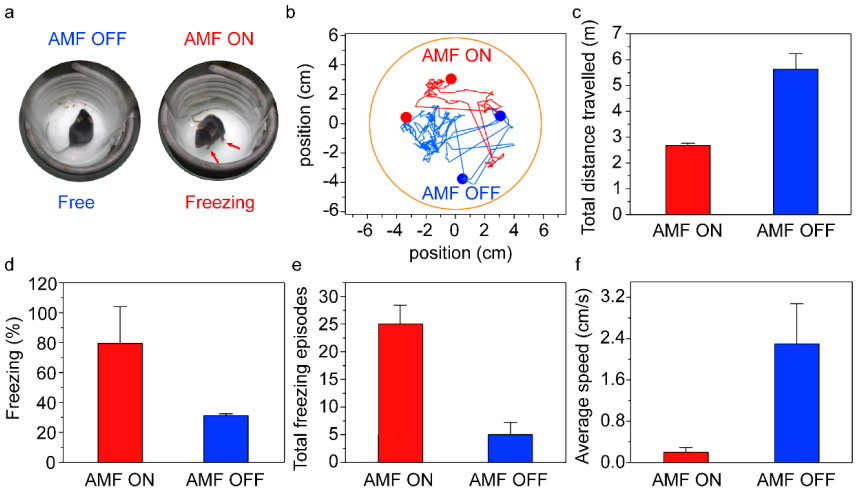

Fig. 6 FVIO-mediated magnetothermal neuromodulation of mouse fear behaviors. (a) A photograph of TRPV1-expressing mouse inside the AMF coil for anti-His-FVIO-based magnetothermal neurostimulation. Behaviors were observed during AMF ON and OFF conditions (20 mT, 275 kHz, 30 s). (b) Example of tracked positions, (c) total distance traveled, (d) percentage of freezing time, (e) total number of freezing episodes, and (f) average speed among the FVIO-treated mice in the AMF coil before (AMF OFF) and during (AMF ON) AMF exposure. The data are presented as the mean ± SEM. The experiments were repeated three times independently.

Long-term magnetothermal neurostimulation in vivo

Το εαλυατε τηε ποτεντιαλ οφ λονγ-τερμ ανδ ρεπεατεδ νευρομοδυλατιον υσινγ Φ″ΙΟς, φεαρ βεηαιορ τεστινγ ιν μιχε ωας χονδυχτεδ οερ 60 δαψς. Ας σηοων ιν Φιγ. 7α, τηε Φ″ΙΟς ρεταινεδ τηε αβιλιτψ το μαγνετοτηερμαλλψ ελιχιτ φρεεζινγ βεηαιορς ιν μιχε ον τηε 60^{τη} δαφ. Ηοωεερ, νο σιγνιφιχαντ χηανγες ιν περχενταγε οφ φρεεζινγ τιμε ωερε οβσερεδ αμονγ τηε ΣΠΙΟ (0.8 μγ)-τρεατεδ μιχε, ωηιχη μαψ βε δυε το ΣΠΙΟ βιοδεγραδατιον ιν τηε ἓΑ. Το χονφιρμ τηις, 7-Τεσλα μαγνετις ρεσονανχε ιμαγινγ (MPI) ωας εμπλοψεδ το εαλυατε τηε χηανγες ιν τηε χονχεντρατιονς οφ τηε μαγνετις νανοηεατερς ιν τηε ἓΑ ρεγιονς ον τηε 1σ^{τ}, 30τη, ανδ 60τη δαψς υσινγ υλτρασηορτ εχηο τιμε (ΥΤΕ) πυλσε σεχυενχες. Λινεαρ χορρελατιονς οφ τηε τρανσερσε ρελαξατιον ρατες ($1/T_2$ αλυες) οφ τηε Φ″ΙΟς ανδ ΣΠΙΟς ωερε φιρστ οβταινεδ (Φιγυρε Σ11, Συππορτινγ Ινφορματιον). Φιγυρε 7β πρεσεντς ΜΡ ιμαγες οφ μουσε βραινς ωιτη ωηιχη τηε χονχεντρατιονς οφ Φ″ΙΟς ανδ ΣΠΙΟς τηατ ρεμαινεδ ιν τηε ἓΑ ρεγιονς χουλδ βε δετερμινεδ (μαρκεδ ωιτη ψελλοω αρροως) ον τηε 1$^{σ\tau}$, 30^{τη}, ανδ 60^{τη} δαψς. Τηε ρελατιε σιγναλ ιντενσιτψ οφ τηε Φ″ΙΟς μεασυρεδ ιν τηε ἓΑ ρεμαινεδ σταβλε φορ 60 δαψς (Φιγυρε 7ς), συγγεστινγ τηατ τηε αμουντ οφ Φ″ΙΟς ρεμαινεδ υνχηανγεδ ατ τηε ινθεχτιον σιτε. Ηοωεερ, τηε ΣΠΙΟ σιγναλ ιν τηε ἓΑ νοταβλψ δεχρεασεδ ον τηε 60^{τη} δαψ, ινδιχατινγ τηειρ δισαππεαρανχε. Τηε δισαππεαρανχε οφ τηε ΣΠΙΟς ις μαινλψ ασχριβεδ το τηειρ σμαλλερ σιζε ιν χομπαρισον ωιτη τηε Φ″ΙΟς, ωηιχη μακες τηειρ βιοδεγραδατιον ανδ diffusion easier. In contrast, the FVIOs were highly stable under physiological conditions, giving them great potential for long-term and repeated neural stimulation and therapy[55].

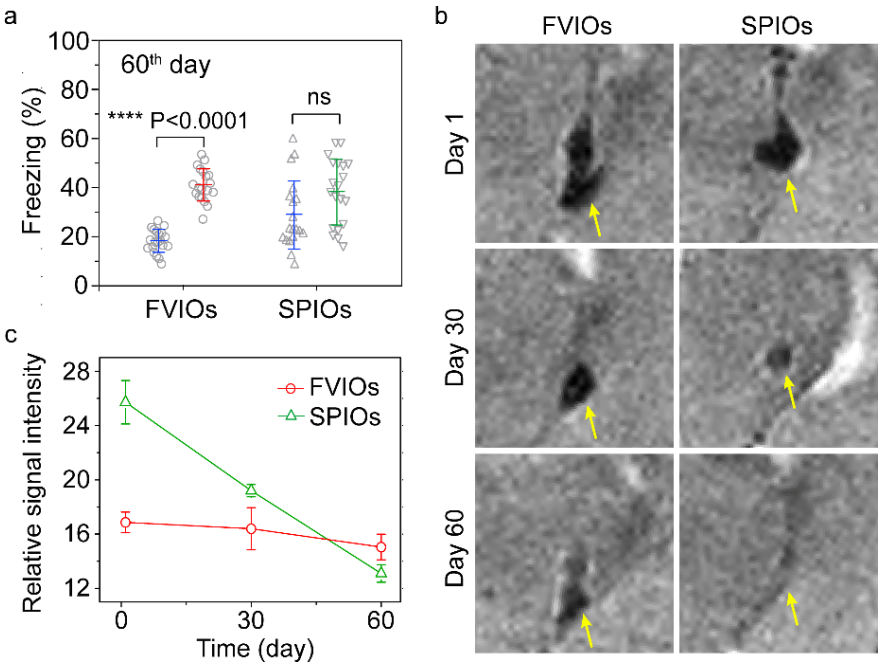

Fig. 7 Long-term magnetothermal neurostimulation mediated by FVIOs. (a) Percentage of freezing time in mice on the 60th day after injection of anti-His-FVIOs (or anti-His-SPIOs) before and after magnetothermal treatment. The data are presented as the means ± SEM. (b) UTE MR images of mouse brains used to evaluate the amount of anti-His-FVIOs (or anti-His-SPIOs) remaining in the CeA regions on the 1st, 30th, and 60th days. (c) Plots of the relative T_2 signal intensity to noise in the CeA regions in the UTE MR images obtained from FVIO- and SPIO-treated mice.

Transgene-free magnetothermal neurostimulation and the induction of fear behaviors

Motivated by the highly efficient activation of neurons in the CeA regions of transgenic TRPV1-expressing mice by the FVIOs, we further explored the possibility of applying this nanoheater to activate endogenous TRPV1-expressing neurons in transgene-free mice. As previously reported, TRPV1 ενδογενουσλψ εξπρεσσεδ ον νευρονς ιν τηε ẽA οφ μιςε[56-57], ωε αλσο ςονφιρμεδ τηε ενδογενους εξπρεσσιον οφ ΤΡΠ″1 (ρεδ) ον ςελλς ιν τηε ẽA ρεγιονς οφ μιςε υσινγ ιμμυνοηιστοςηεμιςαλ μετηοδς, ας σηοων ιν Φιγ. 8α ανδ 8β. Τηεν, τηε Φ″ΙΟς ωερε μοδιφιεδ ωιτη αντι-ΤΡΠ″1 αντιβοδιες το ταργετ ενδογενους ΤΡΠ″1 ιν τηε ẽA ρεγιονς οφ τρανσγενε-φρεε μιςε. Διφφερεντ δοσες οφ αντι-ΤΡΠ″1-Φ″ΙΟς ωερε ινθεςτεδ ιντο τηε ẽA ρεγιονς οφ τηεσε μιςε, ανδ τηε φεαρ βεηαιοραλ ρεσπονσε ινδυςεδ βψ Φ″ΙΟ-μεδιατεδ μαγνετοτηερμαλ στιμυλατιον ωας ινεστιγατεδ υνδερ ΑΜΦ εξποσυρε (20 μΤ, 275 κΗζ). Τηε ρεσυλτς εριφιεδ τηατ τηε αντι-ΤΡΠ″1-Φ″ΙΟς ελιςιτεδ φρεεζινγ βεηαιορς ιν τηε μιςε ατ α μινιμυμ δοσε οφ 0.28 μγ (Φιγυρε 8ς). Τηις τρανσγενε-φρεε μαγνετοτηερμαλ νευροστιμυλατιον στρατεγψ αοιδς ποσσιβλε σιδε εφφεςτς αρισινγ φρομ τηε οερεξπρεσσιον οφ εξογενους ΤΡΠ″1 ανδ γενε δελιερψ ωιτη ιραλ εςτορς, ωηιςη φυρτηερ ιμπροες τηε βιοσαφετψ ανδ εξπανδς τηε σςοπε οφ μαγνετοτηερμαλ νευροστιμυλατιον αππλιςατιονς[11, 58].

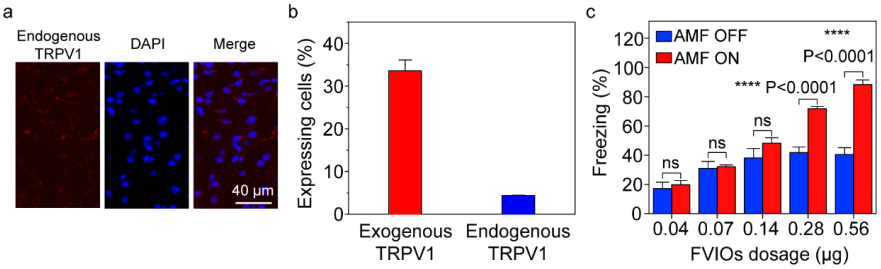

Fig. 8 Transgene-free magnetothermal regulation of fear behaviors in mice using FVIOs. (a) Endogenous TRPV1 expression in the CeA regions of transgene-free mice visualized by immunofluorescence. (b) Quantification of endogenous and exogenous TRPV1 expression in the CeA regions of transgenic and transgene-free mice (n = 4, means ± SEM). (c) Percentage of freezing time in transgene-free mice treated with different doses of FVIOs under AMF exposure (n = 3 to 5, means ± SEM).

Conclusion

In this work, we established the FVIO-mediated magnetothermal neurostimulation technique by systematically investigating the effect of FVIO dose on stimulus-response time and the in vitro and in vivo biosafety, as well as exploring the effectiveness of using this system for long-term, repeated stimulation and magnetothermal regulation in the deep brains of transgene-free mice. Benefiting from the superior heat-generating performance of the FVIOs, anti-His antibody-coated FVIOs triggered Ca^{2+} transients in both transfected 293T cells and cortical neurons at a minimum Fe concentration of 54μγ/μΛ, ωηιςη ωας **20.27-φολδ** λοωερ τηαν τηε Φε ςονςεντρατιον ιν τηε ΣΠΙΟς. Ιν ιο μαγνετοτηερμαλ στιμυλατιον οφ τηε ἒΑ ιν φρεελψ μοινγ μιςε δεμονστρατεδ τηατ τηε μιςε τρεατεδ ωιτη Φ″ΙΟς ατ τηε οπτιμαλ δοσε οφ **0.05** μγ ηαδ a short latency to fear behavior response of approximately **2.51 s** , which was 2.3 times faster than that of the SPIO-treated mice under the same AMF conditions. Furthermore, FVIO-mediated magnetothermal stimulation was safer and allowed long-term control of the freezing behaviors of mice for more than 60 days. Even in nongenetically modified mice, **0.28** μγ of FVIOs was able to activate the endogenous TRPV1 in the CeA and elicit fear behaviors. Overall, we believe that the FVIO-mediated efficient and safe neuromodulation technique established in this study has potential for future neuroscience and therapeutic applications.

MATERIALS AND METHODS

Materials

not-yet-known not-yet-known

not-yet-known

unknown

Synthesis and characterization of FVIOs

Αντιβοδψ βινδινγ: Τηε αντι-Ηις αντιβοδψ ωας ςοαλεντλψ λινκεδ το Φ″ΙΟς ια ΕΔ˜/ΝΗΣ ρεαςτιον. ΔΗ˜Α-Φ″ΙΟς (1 μγ) ωερε ρεαςτεδ ωιτη ΕΔ˜ (10 μΜ) ανδ ΝΗΣ (10 μΜ) φορ 15 μιν ιν ΜΕΣ βυφφερ (0.1 Μ, πΗ 6.0). Τηεν, τηε σολυτιον ωας αδϑυστεδ το πΗ 7.4, ανδ 5 μΛ οφ μουσε μονοςλοναλ αντι-Ηις αντιβοδψ ωας αδδεδ ανδ σηακεν φορ 2 ηουρς. Τηε φιναλ προδυςτς ωερε ωασηεδ ωιτη ΠΒΣ το ρεμοε υνβουνδ αντιβοδιες ανδ δισπερσεδ ιν ΠΒΣ βεφορε ιν ιτρο ανδ ιν ιο τεστινγ.

Characterization: The crystal structure of magnetic nanoheaters was characterized by X-ray diffraction (XRD) patterns using a powder diffractometer (Bruker, D8 Advance, Germany). The morphology

of nanoheaters was observed by scanning electron microscopy (SEM, Hitachi SU8010, Japan). The anti-His antibody-coated nanoheaters were stained with phosphotungstic acid and characterized by transmission electron microscopy (TEM, HT-7700, Japan). The hydrodynamic diameters of nanoheaters were examined by dynamic light scattering (DLS, Malvern, England). The Fe concentration of nanoheater suspensions was detected using inductively coupled plasma mass spectrometry (ICP-MS, Agilent 7900, America). The magnetization curves were determined using a vibrating sample magnetometer (VSM, BKT-4600, China).

Molecular cloning and virus packing

The CMV promoter drives the expression of TRPV1 and mCherry, which was separated by a 2A sequence followed by a stop sequence. TRPV1 DNA fragments inserted with a 6 × His tag were synthesized and cloned into plasmids. The plasmid was packed into the Lenti virus according to established protocols. Before use, all the viral vectors were diluted to a titer of 10^{12} transducing units per milliliter and used for neuronal cell transduction.

Cell culture and transfection

HEK293T cell culture: Before in vitro experiments, the cells were authenticated and checked for mycoplasma contamination. Human embryonic kidney (HEK293T) cells were plated sparsely on culture dishes and cultured in Dulbecco's modified Eagle's medium (DMEM) supplemented with 10% fetal bovine serum (FBS) at 37 **°C** under 5% CO_2. For calcium imaging, the cells were carefully transfected with a certain number of plasmids encoding TRPV1 using 1 μL of a standard transfection reagent (GenEscort^{TM} III) with 2 μg of total DNA. Magnetothermal stimulation was performed one day after transfection of the genetically encoded 293T cells.

Cortical neural cell culture: The whole brain was transferred to PBS containing glucose (33 mM), penicillin-streptomycin (1%, v/v) and washed. The cortical tissues were dissected in a trypsin solution (0.25%, 37 **°C** , 30 min), which was quenched using horse serum (10%, Fisher Scientific) in neurobasal medium. The dissociated tissues were triturated and filtered. The obtained cells were plated onto poly-L-lysine-coated culture dishes. Unattached cells were removed away after 2 h of incubation. The attached cells were cultured in neurobasal medium containing B-27, and half of the medium was replaced every 2 days. Five-day-old cortical neural cells were transfected by adding 2 μL of Lenti-TRPV1-p2A-mCherry (1×10^{12} transducing units/mL). After a 5-day induction period, magnetothermal stimulation was performed for calcium imaging of the TRPV1-expressing cortical neural cells.

Cytotoxicity assay

Cell viability was measured by a CCK-8 assay in 96-well plates. FVIOs at various concentrations (0-1000 μg/mL) were added into each well that seeded with HEK293T cells 24 hours prior. Then, the FVIOs were removed from the culture media. Then, 100 μL of CCK-8 (mg/mL in DMEM) was added into each well and incubated for 2 hours. The absorbance of the supernatant was assayed using a 96-well plate reader at 450 nm.

In vitro magnetothermal stimulation and calcium imaging

Calcium imaging in vitro and fluorescence change quantification were performed as follows. The TRPV1^{His}-expressing HEK293T cells were washed three times in PBS and incubated with Fluo-4 (2 μM) for 30 min at 37 °C. Then, the cells were rewashed with PBS. Next, the anti-His-FVIOs solution (1 mg/mL) was added to the culture medium of TRPV1-expressing cells on a dish for 15 min incubation. The unbound FVIOs in cell culture medium were washed and removed with calcium imaging buffer (105 mM NaCl, 3 mM KCl, 2.5 mM $CaCl_2$, 0.6 mM $MgCl_2$, 10 mM HEPES, 1.2 mM $NaHCO_3$, 100 mM mannitol, and 10 mM glucose) and then imaged in calcium imaging buffer before and during AMF treatment. A magneTherm system with a live-cell coil was employed to provide an AMF at 290 kHz and 20 mT. Calcium fluorescence imaging was performed on a confocal laser microscope (Nikon) system at 20 × magnification. The fluorescence intensities (F_t) during AMF exposure were normalized to the average baseline fluorescence (F_0) to calculate the relative fold change F_t/F_0. The F_0 for each examined cell was obtained for the first 20 seconds before AMF treatment. Responsive

cells and the standard deviations of signals were determined during the stimulation period. The cultured TRPV1^{His}-expressing cortical neurons that bound with FVIOs were also magnetothermally stimulated for calcium imaging experiment as the protocol.

Mice and viral expression in CeA regions

Adult male C57BL/6 mice (6-8 week-old, 20-25 g, Vital River Inc., Beijing, China) were used in this study. Mice were housed 6 per cage in the animal facility and free to food and water. Surgeries including virus and nanoheaters injection were conducted using a standard stereotaxic apparatus under aseptic conditions. The mice were anesthetized through an intraperitoneal injection of pentobarbital sodium (40 mg/kg). Before in vivo magnetothermal neurostimulation, AAV5 virus encoding TRPV1^{His}-mCherry was packaged and injected into CeA region for getting TRPV1^{His}-expressing mice. The stereotaxic coordinate for the CeA was as follows: – 1.25 AP, – 2.75 ML, – 4.30 DV. A small hole was drilled in the skull at the coordinate of CeA and a 32-gauge needle was lowered into the hole. 300 nL of AAV5 virus were injected into the CeA region at 0.1 μL/min using a microsyrine pump. After lifted by 0.1 mm, the syringe was remained for 10 minutes within the brain before slow withdrawal. At least 4 weeks postviral expression, the anti-His-FVIOs in PBS (2 mg/mL) was injected into the same CeA region. The skin tissue was closed with sutures. TRPV1-expressing and FVIOs-loaded mice were prehoused in a closed box with a diameter of 12 cm under a reverse 12-hour light/dark cycle for 3 days as a habituation stage. Animal husbandry and all experimental manipulation of the animals were performed with the approval of the Animal Care and Use Committee of the Chinese Academy of Military Medical Science and Northwest University.

Histology

Histology was used to detect the expression of TRPV1 and c-fos and the successful targeting of anti-His-FVIOs to the TRPV1-expressing neurons. After AMF treatment, the mice were anesthetized and perfused transcardially with PBS and 4% paraformaldehyde (PFA) within 1.5 hours. The isolated brains were fixed in 10% PFA at 4 °C overnight and equilibrated for cryoprotection in 30% sucrose. Coronal brain slices (40 μm thick) were cut on a vibratome. The mouse anti-His tag monoclonal antibody and mouse monoclonal anti-TRPV1 antibody were used in histology. The obtained slices were stained and photographed using a laser-scanning confocal microscope. Confocal images were analyzed using ImageJ software.

Supplementary Materials

Supporting Information is available from the Wiley Online Library or from the author.

The supplementary materials include:

Figures. S1 to S11

Legends for movies S1 to S3

Competing interests

The authors declare that they have no known competing financial interests or personal relationships that could have appeared to influence the work reported in this paper.

REFERENCES

[1] *Nature Reviews Methods Primers* **2022** , 2, 93.[2] M. G. Christiansen, A. W. Senko, P. Anikeeva, *Annu Rev Neurosci* **2019** , 42, 271.[3] M. Roet, S. A. Hescham, A. Jahanshahi, B. P. F. Rutten, P. O. Anikeeva, Y. Temel, *Prog Neurobiol* **2019** , 177, 1.[4] R. Munshi, S. M. Qadri, Q. Zhang, I. Castellanos Rubio, P. del Pino, A. Pralle, *eLife* **2017** , 6, e27069 [5] B. Chen, G. Romero, M. G. Christiansen, A. Mohr, P. Anikeeva, *Science* **2015** , 347(6229), 1477.[6] S. A. Stanley, J. E. Gagner, S. Damanpour, M. Yoshida, J. S. Dordick, J. M. Freidman, *Science* **2012** , 336, 604.[7] R. Munshi, S. M. Qadri, A. Pralle, *Frontiers in Neuroscience* **2018** , 12.[8] H. Huang, S. Delikanli, H. Zeng, D. M. Ferkey, A. Pralle, *Nature Nanotechnology* **2010** , 5, 602.[9] S. A. Stanley, J. Sauer, R. S. Kane, J. S. Dordick, J. M. Friedman, *Nature Medicine* **2015** , 21, 92.[10] S. A. Stanley, L. Kelly, K. N. Latcha, S. F. Schmidt, X. Yu, A. R. Nectow, J. Sauer, J. P. Dyke,

J. S. Dordick, J. M. Friedman, *Nature* **2016** , 531, 647.[11] D. Rosenfeld, A. W. Senko, J. Moon, I. Yick, G. Varnavides, D. Gregurec, F. Koehler, P. H. Chiang, M. G. Christiansen, L. Y. Maeng, A. S. Widge, P. Anikeeva, *Science Advances* **2020** , 6, eaaz3734.[12] X. Long, J. Ye, D. Zhao, S. J. Zhang, *Science Bulletin* **2015** , 60, 2107.[13] C. Sebesta, D. Torres Hinojosa, B. Wang, J. Asfouri, Z. Li, G. Duret, K. Jiang, Z. Xiao, L. Zhang, Q. Zhang, V. L. Colvin, S. M. Goetz, A. V. Peterchev, H. A. Dierick, G. Bao, J. T. Robinson, *Nature Materials* **2022** , DOI: 10.1038/s41563-022-01281-7.[14] B. Torres-Herrero, I. Armenia, M. Alleva, L. Asín, S. Correa, C. Ortiz, Y. Fernández-Afonso, L. Gutiérrez, J. M. de la Fuente, L. Betancor, V. Grazú, *ACS Nano* **2023** , DOI: 10.1021/acsnano.3c01599.[15] A. Tay, D. D. Carlo, *Current Medicinal Chemistry* **2017** , 24, 537.[16] A. M. Zheltikov,*Journal of Applied Physics* **2018** , 123, 224701.[17] C. Yang, S. Park, *Biomedical Engineering Letters* **2021** , 11, 163.[18] L. Signorelli, S.-A. Hescham, A. Pralle, D. Gregurec,*iScience* **2022** , 25, 105401.[19] J. Grandl, S. E. Kim, V. Uzzell, B. Bursulaya, M. Petrus, M. Bandell, A. Patapoutian,*Nat Neurosci* **2010** , 13, 708.[20] W. Gao, Y. Sun, M. Cai, Y. Zhao, W. Cao, Z. Liu, G. Cui, B. Tang, *Nature Communications* **2018** , 9, 231.[21] J. Yao, B. Liu, F. Qin,*Biophysical Journal* **2010** , 99, 1743.[22] M. Barbic,*Elife* **2019** , 8.[23] M. Meister, *Elife* **2016** , 5.[24] X. Yang, E. McGlynn, R. Das, S. P. Paşca, B. Cui, H. Heidari, *Advanced Materials* **2021** , 33, 2103208.[25] G. Romero, M. G. Christiansen, L. Stocche Barbosa, F. Garcia, P. Anikeeva, *Advanced Functional Materials* **2016** , 26, 6471.[26] T. A. Le, M. P. Bui, J. Yoon, *Int J Mol Sci* **2019** , 20.[27] P. Keblinski, D. G. Cahill, A. Bodapati, C. R. Sullivan, T. A. Taton, *Journal of Applied Physics* **2006** , 100, 054305.[28] S. Del Sol-Fernández, P. Martínez-Vicente, P. Gomollón-Zueco, C. Castro-Hinojosa, L. Gutiérrez, R. M. Fratila, M. Moros, *Nanoscale* **2022** , 14, 2091.[29] L. Liu, B. Huang, Y. Lu, Y. Zhao, X. Tang, Y. Shi,*iScience* **2024** , 27, 109201.[30] J. Moon, M. G. Christiansen, S. Rao, C. Marcus, D. C. Bono, D. Rosenfeld, D. Gregurec, G. Varnavides, P. H. Chiang, S. Park, P. Anikeeva, *Advanced Functional Materials* **2020** , 30.[31] M. G. Christiansen, A. W. Senko, P. Anikeeva, *Annual Review Neuroscience* **2019** , 42, 271.[32] X. Lu, G. Li, W. Jiao, K. Li, T. Zhang, X. Liu, H. Fan, *WIREs Nanomedicine and Nanobiotechnology* **2023** , 15, e1890.[33] S. Rao, R. Chen, A. A. LaRocca, M. G. Christiansen, A. W. Senko, C. H. Shi, P. H. Chiang, G. Varnavides, J. Xue, Y. Zhou, S. Park, R. Ding, J. Moon, G. Feng, P. Anikeeva, *Nature Nanotechnology* **2019** , 14, 967.[34] S. Wang, J. Xu, W. Li, S. Sun, S. Gao, Y. Hou, *Chemical Reviews* **2022** , 122, 5411.[35] C. Liang, X. Zhang, Z. Cheng, M. Yang, W. Huang, X. Dong, *VIEW* **2020** , 1, 20200046.[36] H. Gavilán, S. K. Avugadda, T. Fernández-Cabada, N. Soni, M. Cassani, B. T. Mai, R. Chantrell, T. Pellegrino, *Chemical Society Reviews* **2021** , 50, 11614.[37] W. Du, T. Liu, F. Xue, X. Cai, Q. Chen, Y. Zheng, H. Chen, *ACS Appl Mater Interfaces* **2020** , 12, 19285.[38] X. L. Liu, S. Chen, H. Zhang, J. Zhou, H. M. Fan, X. J. Liang, *Adv Mater* **2019** , 31, e1804922.[39] L. Xue, Q. Ye, L. Wu, D. Li, S. Bao, Q. Lu, S. Liu, D. Sun, Z. Sheng, Z. Zhang, N. Gu, J. Sun,*Nano Research* **2023** , 16, 7393.[40] X. Liu, M. Peng, G. Li, Y. Miao, H. Luo, G. Jing, Y. He, C. Zhang, F. Zhang, H. Fan,*Nano Letters* **2019** , 19, 4118.[41] B. Rezaei, P. Yari, S. M. Sanders, H. Wang, V. K. Chugh, S. Liang, S. Mostufa, K. Xu, J.-P. Wang, J. Gómez-Pastora, K. Wu, *Small* **2024** , 20, 2304848.[42] J. Wu, P. Ning, R. Gao, Q. Feng, Y. Shen, Y. Zhang, Y. Li, C. Xu, Y. Qin, G. R. Plaza, Q. Bai, X. Fan, Z. Li, Y. Han, M. S. Lesniak, H. Fan, Y. Cheng, *Advanced Science* **2020** , 7, 1902933.[43] X. Liu, Y. Zhang, Y. Wang, W. Zhu, G. Li, X. Ma, Y. Zhang, S. Chen, S. Tiwari, K. Shi, S. Zhang, H. M. Fan, Y. X. Zhao, X.-J. Liang, *Theranostics* **2020** , 10, 3793.[44] X. Liu, Y. Zhang, Y. Guo, W. Jiao, X. Gao, W. S. V. Lee, Y. Wang, X. Deng, Y. He, J. Jiao, C. Zhang, G. Hu, X.-J. Liang, H. Fan, *Advanced Science* **2021** , 8, 2100950.[45] X. Liu, M. Peng, G. Li, Y. Miao, H. Luo, G. Jing, Y. He, C. Zhang, F. Zhang, H. Fan, *Nano Lett* **2019** , 19, 4118.[46] X. Li, H. Xiong, N. Rommelfanger, X. Xu, J. Youn, P. A. Slesinger, G. Hong, Z. Qin, *Matter* **2021** , 4, 1484.[47] E. Kosari, K. Vafai, *Brain Multiphysics* **2020** , 1, 100014.[48] H. Liu, R. Sun, L. Wang, X. Chen, G. Li, Y. Cheng, G. Zhai, B.-H. Bay, F. Yang, N. Gu, Y. Guo, H. Fan, *ACS Nano* **2022** , 16, 18806.[49] T. Zhang, G. Li, Y. Miao, J. Lu, N. Gong, Y. Zhang, Y. Sun, Y. He, M. Peng, X. Liu, X.-J. Liang, H. Fan, *Biomaterials* **2021** , 276, 121021.[50] X. L. Liu, Y. Yang, C. T. Ng, L. Y. Zhao, Y. Zhang, B. H. Bay, H. M. Fan, J. Ding, *Adv Mater* **2015** , 27, 1939.[51] J. M. Moscarello, M. A. Penzo, *Nature Neuroscience* **2022** , 25, 999.[52] T. Yang, K. Yu, X. Zhang, X. Xiao, X. Chen, Y. Fu, B. Li,*Nature* **2023** , 616, 510.[53] H. M. Fahmy, E. M. Aly, F. F. Mohamed, N. A. Noor, A. A. Elsayed, *NeuroToxicology* **2020** , 77, 80.[54] S. Nimpf, D. A. Keays, *The EMBO Journal* **2017** , 36, 1643.[55] F. Benfenati, G. Lanzani,*Nature Reviews Materials* **2020** , 6, 1.[56] S. J. McDougall, H. Guo, M. C. Andresen, *The Journal of Physiology* **2017** , 595, 901.[57] M. Aurélie, B. Mathieu, *The Journal of*

Neuroscience **2011** , 31, 13025.[58] Z. Zhang, Y. You, M. Ge, H. Lin, J. Shi, *Journal of Nanobiotechnology* **2023** , 21, 319.